

# FAST ALGORITHMS FOR FOURIER EXTENSION BASED ON BOUNDARY INTERVAL DATA \*

ZHENYU ZHAO<sup>†</sup>, YANFEI WANG<sup>‡</sup>, AND ANATOLY G. YAGOLA<sup>§</sup>

**Abstract.** In this paper, we first propose a new algorithm for the computation of Fourier extension based on data near the two endpoints of the interval, which can obtain an effective Fourier series approximation for non-periodic functions. The algorithm calculates the extended part using the boundary interval data and then combines it with the original data to form the data of the extended function within a period. By testing the key parameters involved, their influence on the algorithm was clarified and an optimization setting scheme for the parameters was proposed. Compared with FFT, the algorithm only needs to increase the computational complexity by a small amount. Then, an improved algorithm for the boundary oscillation function is proposed. By refining the boundary interval grid, the resolution constant of the boundary oscillation function was reduced to approximately 1/4 of the original method.

**Key words.** Fourier Series, Fourier Extensions, Fourier Continuation, Resolution Constant

**AMS subject classifications.** 42A10, 65T40, 65T50

**1. Introduction.** Fourier series approximation has been widely used in various fields for smooth periodic functions. In many physical, engineering and exploration geophysical problems, such as analyzing periodic signals in electrical engineering, studying periodic motion in mechanics such as the oscillation of a pendulum under certain ideal conditions, or decomposing seismic/electromagnetic signals into different frequency components using Fourier series approximation [17, 19, 20]. The Fourier series approximation offers spectral convergence since more terms are added to the Fourier series, the approximation converges to the actual function in an efficient way in the frequency domain. Moreover, it can be computed numerically via the FFT (Fast Fourier Transform), which is a computationally efficient algorithm. However, the situation changes completely once the periodicity is lost. A jump discontinuity is imposed in the approximation at the domain boundaries, owing to the well-known Gibbs phenomenon. For instance, when we attempt to approximate a function that is not periodic over a given interval using Fourier series, we will observe this Gibbs phenomenon near the boundaries of the interval. Several methods have been developed to ameliorate the ill effects of the Gibbs phenomenon. For example, methods based on Gegenbauer polynomials, which have certain orthogonality properties that can be exploited to obtain better approximate functions [9, 10, 18]. Methods utilizing Padé approximations, which are rational function approximations, can also be used [7, 8]. And Fourier extension (or continuation) methods, which extend the function in a certain way to make it more suitable for Fourier-based approximation, are also among the approaches developed to address this problem [4, 6, 11, 12, 13, 14, 15, 21].

The idea of the existing discrete Fourier extension can be described as follows: Let  $f$  be a non-periodic, smooth and sufficiently differentiable function over  $[-1, 1]$ ,

---

\*The research is partially supported by National Natural Science Foundation of China (No. 12171455, RSF-NSFC 23-41-00002)

<sup>†</sup>School of Mathematics and Statistics, Shandong University of Technology, Zibo, 255049, China, (Zhenyu.Zhao@sdut.edu.cn).

<sup>‡</sup>State Key Laboratory of Deep Petroleum Intelligent Exploration and Development, Institute of Geology and Geophysics, Chinese Academy of Sciences, Beijing, 100029, China, (yfwang@mail.iggcas.ac.cn).

<sup>§</sup>Department of Mathematics, Faculty of Physics, Lomonosov Moscow State University, Vorobyevy Gory, 119991 Moscow, Russia, (yagola@physics.msu.ru)

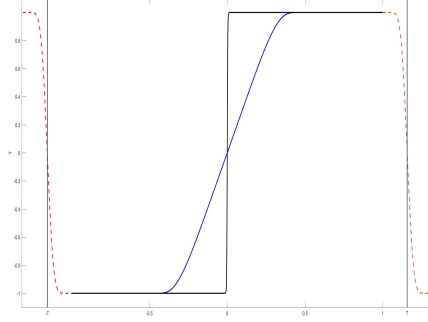


FIG. 1.1. Periodic extensions of  $f_1(t)$  and  $f_2(t)$ .

which is sampled in a predefined set of points  $\{t_\ell\} \subset [-1, 1]$ , the discrete Fourier extension  $C(f)$  of  $f$  is defined by

$$C(f) = \sum_{k=-N}^N \mathbf{c}_k e^{i \frac{k\pi}{T} t}, \quad T > 1, \quad (1.1)$$

where the coefficients  $\{\mathbf{c}_k\}_{k=-N}^N$  are chosen to minimize the error

$$\min \sum_{\ell} \left| f(t_\ell) - \sum_{k=-N}^N \mathbf{c}_k e^{i \frac{k\pi}{T} t_\ell} \right|^2. \quad (1.2)$$

To obtain a solution to the minimization problem (1.2), a severely ill-conditioned least-squares system has to be solved. In [4], Boyd introduced truncated singular value decomposition (TSVD) to stabilize the calculation process, with an accuracy almost up to machine precision. A convergence analysis by Adcock et al. states that for analytic functions the method is at least superalgebraically convergent [2]. Utilizing randomized algorithms, Lyon provided a fast algorithm with  $T = 2$  [12]. In [14], Matthysen et al. presented fast algorithms for arbitrary  $T$ , exploiting it as a specific variant of bandlimited extrapolation. This idea was further developed in [15] to form a fast algorithm for function approximation in 2D domains.

It should be noted that the goal of the extension process is to effectively connect the data at both ends of the function. The following two functions were constructed:

$$f_1(t) = \begin{cases} -1, & x < -\frac{1}{2}, \\ \tanh(\tan \pi t), & -\frac{1}{2} \leq t \leq \frac{1}{2}, \\ 1, & t > \frac{1}{2}, \end{cases} \quad (1.3)$$

$$f_2(t) = \begin{cases} -1, & t < -\frac{1}{2}, \\ \tanh(100 \tan \pi t), & -\frac{1}{2} \leq t \leq \frac{1}{2}, \\ 1, & t > \frac{1}{2}. \end{cases}$$

Because the data of the two functions near the endpoints are the same, the same connection data can be used in the intervals  $[-T, 1)$  and  $(1, T]$ . An illustration of this process is shown in Fig. 1.1. This raises the issue of whether the data inside the interval really help in the calculation of the extension. In fact, a very efficient method, known as the FC-Gram method has been developed earlier, which uses only boundary data (projecting it into a basis of orthogonal polynomials) for extension calculations [5]. Recently, this method has also been extended to the approximation of two-dimensional functions[6]. In [16], the authors proposed a method to calculate the Fourier extension using the derivative on the boundary combined with a two-point Taylor interpolation polynomial. The extension part calculated by these two methods are more stable, but neither of them is superalgebraically convergent because polynomials need to be introduced. Judging from the numerical results given in the literature, the number of nodes required by these two methods was significantly higher than that of the previous method when obtaining the same accuracy. In [5], the authors identified a critical limitation in directly applying the original extension algorithm with relatively few nodes in the boundary interval: the inherent difficulty in achieving satisfactory approximation accuracy. Therefore, they turned to precede the FC(SVD) calculation by projecting them into the bases of orthogonal polynomials. However, existing theoretical analyses reveal that the accuracy of the Fourier extension is co-determined by two interdependent parameters –extension length and sampling ratio. In previous studies, researchers tended to increase the sampling ratio to improve accuracy. This is because in the full data algorithm, increasing the extension length does not seem to bring any benefits. In this study, we will point out that by increasing the extension length, the number of nodes required in the boundary interval can be effectively reduced. Specifically, we demonstrate that through optimal parameter combinations, an accurate extension computation can be achieved with a few boundary nodes deployment. The number of nodes required in the boundary interval can be fixed, and is only related to the desired accuracy.

In this paper, we first propose a new fast algorithm for the calculation of the Fourier extension, which has the following traits:

- By optimizing the parameter settings, only a few nodes in the boundary interval are required to calculate the extension part; Thus, the method can be computed with FFT speed. Unlike the FC-Gram algorithm, the method does not require the introduction of polynomials. When the behavior of the boundary is not significantly better than that of the interior, the proposed algorithm requires significantly fewer nodes than the FC-Gram algorithm because it maintains the superalgebraic convergence property of the original algorithm.
- Because the calculation of the extension part uses only the data of the small interval near the boundary, the influence of oscillations within the interval on the approximation is significantly weakened. Therefore, for a function that is smooth in the neighborhood of the interval boundary and oscillates within the interval, the proposed algorithm has a smaller resolution constant than that of the original full-data algorithm. This also applies to the FC-Gram algorithm.

Furthermore, for functions that oscillate in the neighborhood of the interval boundary, we propose an improved algorithm based on boundary interval grid refinement, which can significantly reduce the resolution constant of this type of function. The proposed algorithms exhibit good performance and provide clear conclusions

regarding the settings of various parameters. Therefore, we believe that it is of substantial interest to those who use FEs in practice.

**1.1. Overview of the paper.** In Section 2, we outline the algorithm and explain its structure. The specific calculation method of the extension part based on boundary interval data is presented in Section 3. Section 4 present the computational complexity and resolution constant analysis of the algorithm. In Section 5, we systematically tests the key parameters, identifies their influencing factors, and provide an optimization setting scheme. In Section 6, we present numerical tests of the final algorithm and compare it with three other fast algorithms. Furthermore, for the boundary oscillation function, we propose an improved algorithm based on the boundary interval grid refinement.

**2. Outline of the boundary interval algorithm.** In this paper, we restrict ourselves to the case where the sampling points are uniform, that is,

$$t_\ell = \frac{\ell}{M}, \quad \ell = -M, \dots, M. \quad (2.1)$$

Let the positive integer  $m_\Delta$  be the number of nodes taken in the boundary interval, and  $S_l, S_r$  be the set of corresponding subscripts,

$$S_l = \{-M, -M+1, \dots, -M+m_\Delta-1\}, \quad S_r = \{M-m_\Delta+1, M-m_\Delta+2, \dots, M\}. \quad (2.2)$$

Let  $T_\Delta > 1$  and

$$L_\Delta = 2 \times \lceil T_\Delta \times (m_\Delta - 1) \rceil, \quad h = \frac{2\pi}{L_\Delta}, \quad x_j = (j-1)h, \quad j = 1, 2, \dots, L_\Delta, \quad (2.3)$$

where  $\lceil \cdot \rceil$  is the rounding symbol. Then let

$$J_{\Delta,1} = \{1, 2, \dots, m_\Delta\}, \quad J_{\Delta,2} = \left\{ \frac{L_\Delta}{2} + 1, \frac{L_\Delta}{2} + 2, \dots, \frac{L_\Delta}{2} + m_\Delta \right\}, \quad J_\Delta = J_{\Delta,1} \cup J_{\Delta,2}. \quad (2.4)$$

For  $j \in J_\Delta$ , take

$$g(x_j) = \begin{cases} f(t_{M-m_\Delta+j}), & j \in J_{\Delta,1}, \\ f(t_{-M+j-L_\Delta/2-1}), & j \in J_{\Delta,2}. \end{cases} \quad (2.5)$$

Then we calculate the extension function  $g_c$  defined on the interval  $[0, 2\pi]$  of  $g$ , and obtain its values at  $x_j, j = 1, 2, \dots, L_\Delta$  according to the method described in Section ???. Finally, we obtain the function  $f_c$  with a period of  $2 + \lambda$ , where

$$\lambda = \frac{\lceil T_\Delta - 1 \rceil \times (m_\Delta - 1)}{M}, \quad (2.6)$$

and the data of the extension function  $f_c(t_\ell), \ell = -M, \dots, M, M+1, \dots, M + \frac{L_\Delta}{2} - m_\Delta$  in one period  $[-1, 1 + \lambda)$  is

$$f_c(t_\ell) = \begin{cases} f(t_\ell), & |\ell| \leq M, \\ g_c(x_{m_\Delta+\ell-M}), & \ell > M. \end{cases} \quad (2.7)$$

Fig. 2.1 shows the basic process of the boundary interval algorithm using the function  $f(x) = x^2$  as an example. Here, to make the graph clearer, we use a relatively

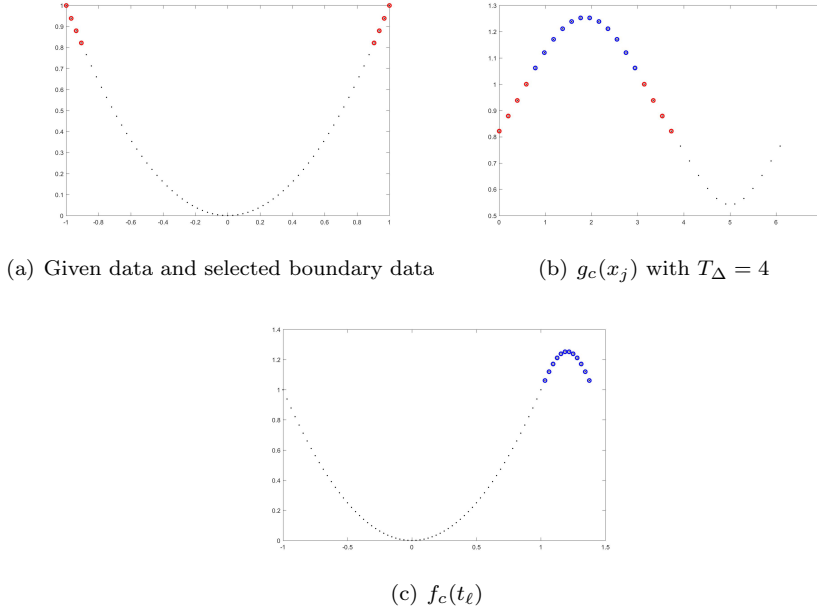


FIG. 2.1. Calculation process of a periodic extension of  $f(x) = x^2$ .

small number of nodes. Fig. 2.1(a) shows the given data (indicated by the black dotted line) and boundary data selected for the calculation extension (indicated by the red circle). Fig. 2.1(b) shows the  $g_c(x_j)$  calculated from the boundary data. The data represented by blue circles represent the subsequent extension data required. Fig. 2.1(c) shows the data of  $f_c$  in one period formed by combining the original data with the calculated extension data. It can be observed from the calculation process that the calculation of the extension part depends only on the boundary interval data.

After obtaining the data in one period, the subsequent algorithm can be implemented using FFT. Therefore, whether the algorithm can achieve satisfactory efficiency depends on the computational complexity of the extension part, that is, the size of the parameters  $T_\Delta$  and  $m_\Delta$ . We present their selection schemes through testing in Section 5.

**3. The calculation of  $g_c$ .** Including the appropriate normalization, we let

$$\phi_k(x) = \frac{1}{\sqrt{L_\Delta}} e^{ikx}, \quad k = -n_\Delta, \dots, n_\Delta, \quad x \in [0, 2\pi]. \quad (3.1)$$

Assuming  $g(x_j)$  is given by (2.5), then the extension function  $g_c$  of  $g$  is defined as

$$g_c(x) = \sum_{k=-n_\Delta}^{n_\Delta} \mathbf{c}_k \phi_k(x). \quad (3.2)$$

where the coefficients  $\mathbf{c}_k$  are determined by

$$\min_{(\mathbf{c}_k)} \sum_{j \in J_\Delta} \left| \sum_{k=-n_\Delta}^{n_\Delta} \mathbf{c}_k \phi_k(x_j) - g(x_j) \right|^2. \quad (3.3)$$

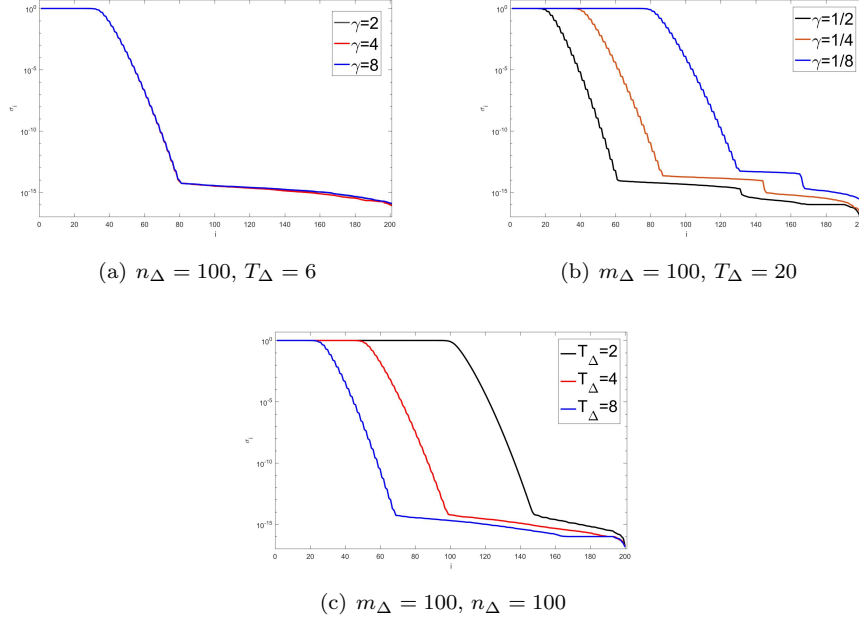


FIG. 3.1. The singular values of  $A$  for various  $m_\Delta$ ,  $n_\Delta$  and  $T_\Delta$ .

If we let

$$\begin{aligned}
 A_{l,k} &= \begin{cases} \phi_k(x_l), & 1 \leq l \leq m_\Delta, \\ \phi_k(x_{\frac{L_\Delta}{2} + l - m_\Delta}), & m_\Delta < l \leq 2m_\Delta, \end{cases} \\
 b_l &= \begin{cases} \frac{1}{m_\Delta} f(x_l), & 1 \leq l \leq m_\Delta, \\ \frac{1}{m_\Delta} f(x_{\frac{L_\Delta}{2} + l - m_\Delta}), & m_\Delta < l \leq 2m_\Delta, \end{cases} \\
 l &= 1, 2, \dots, 2m_\Delta, k = -n_\Delta, \dots, n_\Delta.
 \end{aligned} \tag{3.4}$$

Then the solution of (3.3) can be obtained by solving the rectangular system

$$Ac \approx b \tag{3.5}$$

in a least squares sense. If we let

$$N_\Delta = \min\{2m_\Delta, 2n_\Delta + 1\}, \tag{3.6}$$

then the SVD of  $A$  can be given as

$$A = \sum_{i=1}^{N_\Delta} \mathbf{u}_i \sigma_i \mathbf{v}_i^T, \tag{3.7}$$

where  $\sigma_i$  are the singular values of  $A$  such that

$$\sigma_1 \geq \dots \geq \sigma_{N_\Delta} \geq 0, \tag{3.8}$$

while  $\mathbf{u}_i$  and  $\mathbf{v}_i$  are the left and right singular vectors of  $A$ , respectively. We define

$$\gamma_\Delta = \frac{m_\Delta - 1}{n_\Delta}. \quad (3.9)$$

Fig. 3.1 shows the singular values of  $A$  calculated by SVD techniques for various  $m_\Delta$ ,  $n_\Delta$  and  $T_\Delta$  in MATLAB. It can be observed that the first approximately  $\mathcal{O}(n_\Delta/T_\Delta)$  are close to 1 and then the singular values rapidly decay until the true singular values are masked by machine precision errors.

The situation of singular values reflects the ill-posedness of (3.5), regularization must be introduced. Referring to the treatment methods in [2], the truncated SVD least-squares solution to (3.5) can be given as

$$\mathbf{c}_\tau = \sum_{\sigma_i > \tau} \frac{\mathbf{u}_i^T \mathbf{b}}{\sigma_i} \mathbf{v}_i, \quad (3.10)$$

where parameter  $\tau$  is usually chosen to be close to the machine precision.

**4. Computational complexity and resolution constant .** The computational complexity of the proposed algorithm comprises three parts:

- **Calculation of  $\mathbf{c}_\tau$ .** The computational effort in this step is mainly concentrated on the singular value decomposition of matrix  $A$ , which is related to  $m_\Delta$  and  $\gamma$ , and can be estimated as

- If  $\gamma_\Delta < 1$ , the computational complexity is

$$\mathcal{O}(m_\Delta^2 n_\Delta) = \mathcal{O}\left(\frac{1}{\gamma_\Delta} m_\Delta^3\right). \quad (4.1)$$

- If  $\gamma \geq 1$ , the computational complexity is

$$\mathcal{O}(m_\Delta n_\Delta^2) = \mathcal{O}\left(\frac{1}{\gamma_\Delta^2} m_\Delta^3\right). \quad (4.2)$$

- **Calculation of  $g_c$ .** This step can be achieved by IFFT, the computational complexity is

$$\mathcal{O}(L_\Delta \log(L_\Delta)). \quad (4.3)$$

- **Calculation of Fourier coefficients of  $f_c$ .** This can be achieved by FFT, and the computational complexity is

$$\mathcal{O}(M \log(M)). \quad (4.4)$$

Next, we analyze the factors that affect these parameters in detail. First, we provide the following concept for the resolution constant, which comes from the literature [3]:

**DEFINITION 4.1.** Let  $\{F_M\}_{M \in \mathbb{N}}$  be a sequence of approximations such that  $F_M(f)$  depends only on the values of  $f$  on an equispaced grid of  $2M + 1$  points. Let

$$\mathcal{R}(\omega, \delta) = \min \{M \in \mathbb{N} : \|\exp(i\pi\omega t) - F_M(\exp(i\pi\omega t))\|_\infty \leq \delta\}, \quad \omega > 0, \quad 0 < \delta < 1,$$

then we say that  $F_M$  has resolution constant  $0 < r < \infty$  if

$$R(\omega, \delta) \sim r\omega, \omega \rightarrow \infty, \quad (4.5)$$

for any fixed  $\delta$ .

The resolution constant of the present method is influenced by two aspects:

- First, we need to consider the approximation ability of  $g_c$  to the boundary interval data of the function  $f$ . For the function  $f(x) = \exp(i\pi\omega t)$  on  $[-1, 1]$ , since the calculation of  $g_c$  is performed on  $[0, 2\pi]$  after intercepting the boundary interval data, the function corresponding to  $g$  in (2.5) is

$$g(x) = \exp(i\omega_\Delta \pi t),$$

where

$$\omega_\Delta = \frac{m_\Delta - 1}{M} T_\Delta \omega. \quad (4.6)$$

Obviously, if  $g_c$  is to be able to effectively approximate  $g$ , it must satisfy

$$n_\Delta \geq \omega_\Delta. \quad (4.7)$$

Therefore, according to (4.6), (4.7) and (3.9), it can be obtained that the number of nodes  $M$  have to satisfy

$$M \geq \gamma_\Delta T_\Delta \omega. \quad (4.8)$$

- Second, it is necessary to consider the number of nodes required for using  $f_c$  to calculate the overall approximation. In this step we use FFT to approximate a periodic function, according to the basic conclusion of Fourier approximation, this step requires the number of nodes  $M$  to satisfy

$$M \geq \omega. \quad (4.9)$$

Note that in the above analysis process, we consider the case where the internal and boundary frequencies are the same. In the actual calculation process, when facing general functions, it can be seen from the above analysis that if the frequency of the function at the boundary is significantly lower than that of the interior, the number of nodes required for calculation will be greatly reduced. This also applies to the FC-Gram algorithm. We will verify this in the subsequent numerical experiments.

Through (4.1)-(4.3) and the above analysis, we can see that whether the proposed method can have a smaller computational complexity depends on whether there is a smaller  $m_\Delta$  value that can enable  $g_c$  to accurately approximate the function in the boundary interval. In the original full-data Fourier extension algorithm, most literatures recommend the use of oversampling mode. The results show that the accuracy of the calculation can be improved with the increase of the sampling ratio

$$\gamma = \frac{M}{N}.$$

In fact, the increase of  $\gamma$  plays a role in reducing the discrete step length on  $[-T, T]$ , which can also be achieved by increasing  $T$ , as mentioned in the previous literature on the estimation of the resolution constant of the full-data algorithm [3]:

$$r \sim T\gamma. \quad (4.10)$$

In previous studies on full-data algorithms, researcher tend to increase  $\gamma$  because no benefits were observed with increasing  $T$ . However, for the algorithm proposed in this paper, increasing  $T$  seems to be a better choice because it significantly reduces the number of nodes required for the boundary interval. In the next section, we will test these parameters more comprehensively and provide clear results and parameter setting suggestions, so that the algorithm can complete the calculation with lower computational complexity.



TABLE 5.1  
The approximation value of  $\hat{T}_1$  for various  $\gamma$ .

$\gamma$	8	4	2	1	$\frac{1}{2}$	$\frac{1}{4}$	$\frac{1}{8}$
$\hat{T}_1$	1.09	1.20	2.3	5.9	12.5	24.6	48.9

**5. Numerical investigation and determination of key parameters.** The proposed algorithm involves multiple parameters, and their selection has a substantial influence on the performance of the algorithm. This section tests and analyzes them and then provides an optimized scheme.

**5.1. Testing the parameter  $T_\Delta$ .** From the analysis in the previous section, we know that the extension length  $T_\Delta$  has a substantial influence on the convergence rate and the resolution power. Generally, a larger extension length can achieve a higher convergence rate but also means a larger resolution constant.

In this section, we numerically observe the impact of  $T_\Delta$  on the performance of the algorithm. Now we take

$$f(t) = \exp(i\pi\omega t)$$

to test the interaction between  $T_\Delta$  and the other parameters. In Fig 5.1, we present the results of the approximation error against  $T_\Delta$  for different parameters. Here and what follows, the approximation error is evaluated as the maximum pointwise error over an equi-sampled grid that is ten times denser than that used for construction and the parameter  $\tau = 1e - 14$  (we also tested with  $\tau = 1e - 12, 1e - 13, 1e - 15$  and obtained results similar to those shown here.) Three distinct regions are visible in all graphs in Fig. 5.1:

- Region  $I_1 := \{T_\Delta : 1 < T_\Delta < \hat{T}_1\}$ , where the error decreases rapidly to the machine accuracy as  $T_\Delta$  increases.
- Region  $I_2 := \{T_\Delta : \hat{T}_1 < T_\Delta < \hat{T}_2\}$ , where the error is maintained close to the machine accuracy.
- Region  $I_3 := \{T_\Delta > \hat{T}_2\}$ , where the error rebounds, and the increase in  $T_\Delta$  causes the error to increase instead.

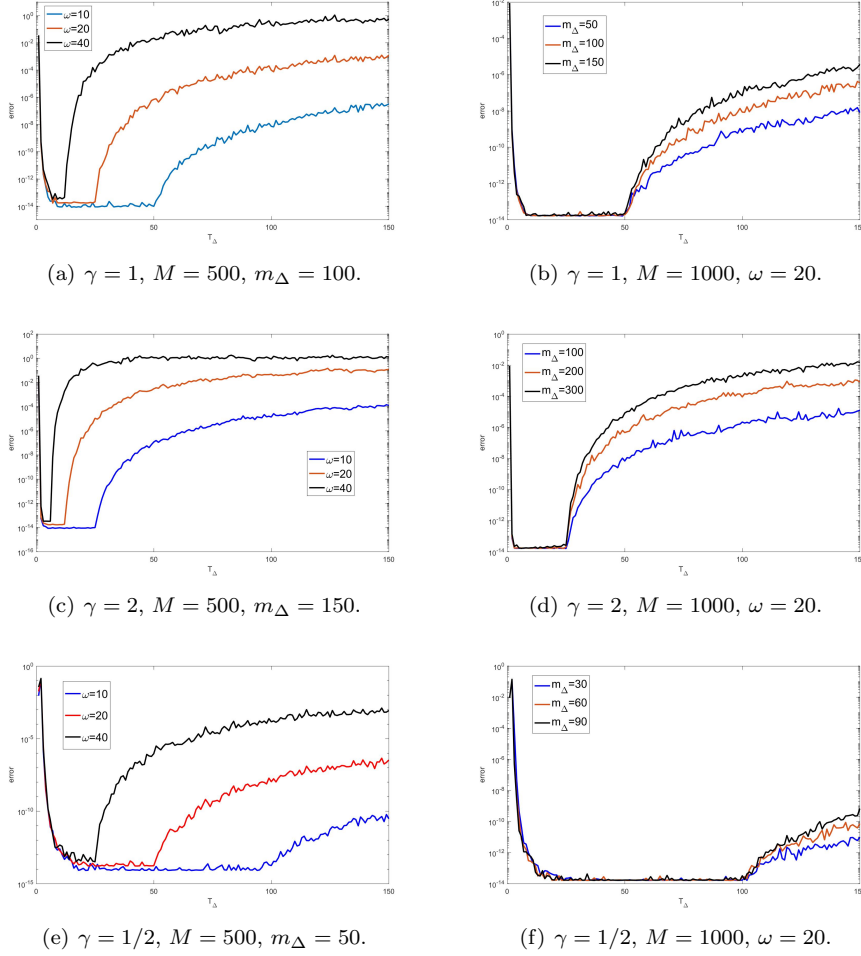
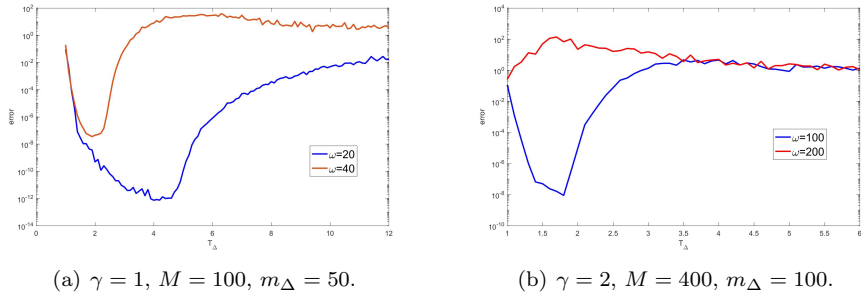
It can be seen that the value of  $\hat{T}_1$  is influenced by  $\gamma_\Delta$ , but not by  $\omega$ ,  $m_\Delta$ , and  $M$ , while  $\hat{T}_2$  is influenced by  $\gamma_\Delta$ ,  $M$ , and  $\omega$ . For several different values of  $\gamma_\Delta$ , we give the approximate values of  $\hat{T}_1$  (we tested the functions of  $\omega$  from 1 to 50, and took the mean of the corresponding  $T_\Delta$  when their error was less than  $1e - 13$  for the first time as the estimate of  $\hat{T}_1$ ), which are listed in Table 5.1. For  $\hat{T}_2$ , we can estimate:

$$\hat{T}_2 \sim \frac{M}{\gamma_\Delta \omega}. \quad (5.1)$$

This is consistent with the result obtained in equation (4.8).

When the number of nodes  $M$  is not sufficiently large, regions  $I_1$  and  $I_2$  are merged into a single region. At this time, the error reached the optimal value near  $\hat{T}_2$ . This phenomenon is shown in Fig. 5.2.

What will happen if the  $T_\Delta$  value selected is less than  $\hat{T}_1$ ? Figure 5.3 shows this. We can see that the error will not decrease after reaching a certain threshold, which cannot be improved by increasing the numbers of  $M$  and  $m_\Delta$ . It should be noted that this situation also applies to the Fourier extension algorithm using the full data in

FIG. 5.1. The approximation error against  $T_{\Delta}$  for various parameters.FIG. 5.2. The approximation error against  $T_{\Delta}$  for  $\hat{T}_2 < \hat{T}_1$ .

previous literatures. In Fig. 5.4, we show the results of the algorithm using full data. It can be seen that when  $\gamma$  is fixed and the value of  $T$  is smaller than the corresponding  $\hat{T}_1$ , the method cannot achieve machine accuracy. Similarly, this cannot be improved by increasing the number of  $M$ .

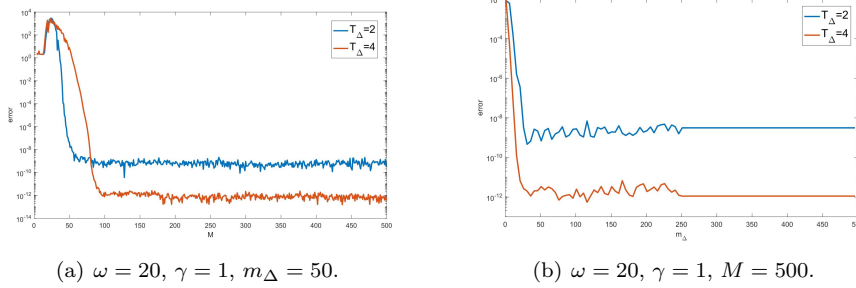


FIG. 5.3. The approximation error against  $T_\Delta$  for  $T_\Delta < \hat{T}_1$  (If  $m_\Delta > M$ , we take  $m_\Delta = M$ ).

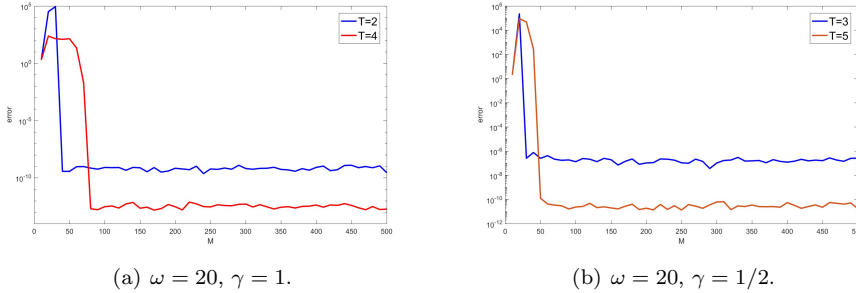
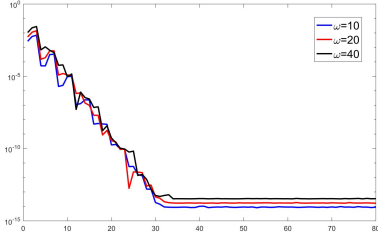
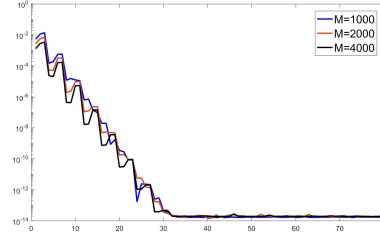
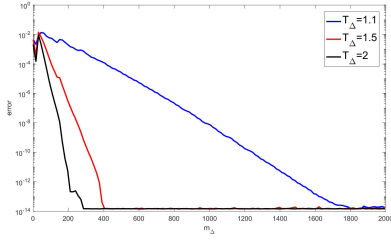
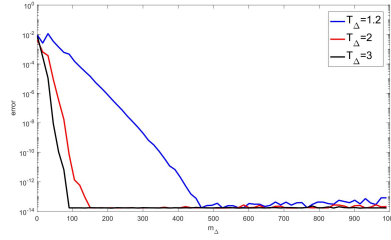
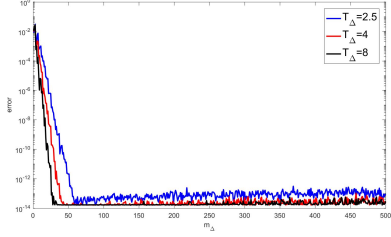
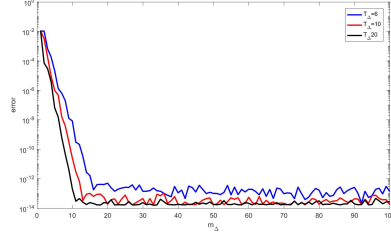
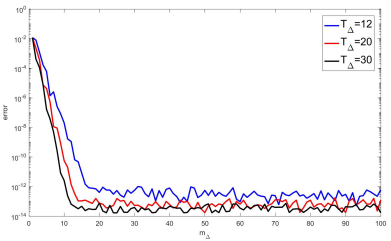
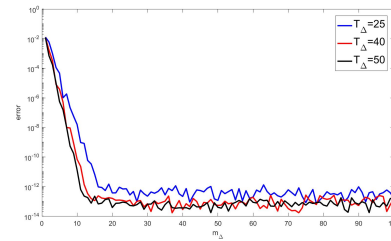


FIG. 5.4. The approximation error against  $M$  for full data FE with  $T < \hat{T}_1$ .

From the test results above, we can see that when  $\gamma_\Delta$  is fixed, the selection of  $T_\Delta$  is crucial to the approximation accuracy. The approximation can obtain satisfactory results only when  $T_\Delta$  is within the interval  $[\hat{T}_1, \hat{T}_2]$ . The left endpoint  $\hat{T}_1$  of the interval is determined by parameter  $\gamma_\Delta$ , whereas the right endpoint  $\hat{T}_2$  is affected by parameters  $\gamma_\Delta, \omega$  and  $M$ .

**5.2. Testing the parameter  $m_\Delta$ .** The size of the parameter  $m_\Delta$  determines whether this study is meaningful. This subsection tests the influence of the other parameters on it. First, we take  $M > T_\Delta \gamma_\Delta \omega$  for observation. As shown in Fig. 5.5, as the value of  $m_\Delta$  increases, the error decreases rapidly and reaches the machine precision after a certain value  $\hat{m}_\Delta$ , while the value of  $\hat{m}_\Delta$  is independent of  $M$  and  $\omega$ .

(a)  $M = 1000$ ,  $\gamma_\Delta = 2$ ,  $T_\Delta = 6$ .(b)  $\omega = 20$ ,  $\gamma_\Delta = 2$ ,  $T_\Delta = 6$ .FIG. 5.5. The approximation error against  $m_\Delta$  for various  $\omega$  and  $M$ .(a)  $M = 2000$ ,  $\gamma_\Delta = 8$ ,  $\omega = 20$ .(b)  $M = 1000$ ,  $\gamma_\Delta = 4$ ,  $\omega = 20$ .(c)  $M = 500$ ,  $\gamma_\Delta = 2$ ,  $\omega = 20$ .(d)  $M = 500$ ,  $\gamma_\Delta = 1$ ,  $\omega = 20$ .(e)  $M = 500$ ,  $\gamma_\Delta = 1/2$ ,  $\omega = 20$ .(f)  $M = 500$ ,  $\gamma_\Delta = 1/4$ ,  $\omega = 20$ .FIG. 5.6. The approximation error against  $m_\Delta$  for various  $\gamma_\Delta$  and  $T_\Delta$ .

In Fig. 5.6, we further show how the error changes with  $m_\Delta$  for different values of  $\gamma_\Delta$  and  $T_\Delta$ . It can be seen that the value of  $\hat{m}_\Delta$  decreases with the increase of  $T_\Delta$ . This is consistent with the previous analysis, because the step size  $h = \frac{2\pi}{L_\Delta}$  in the  $g_c$

TABLE 5.2  
The approximation values of  $\hat{m}_\Delta$  for various  $\gamma$  and  $T_\Delta$ .

$\gamma_\Delta$	8	4	2	1	$\frac{1}{2}$	$\frac{1}{4}$	$\frac{1}{8}$
$T_\Delta$	1.1	1.2	2.3	6	12	24	50
$\hat{m}_\Delta$	1870	490	64	23	25	24	26

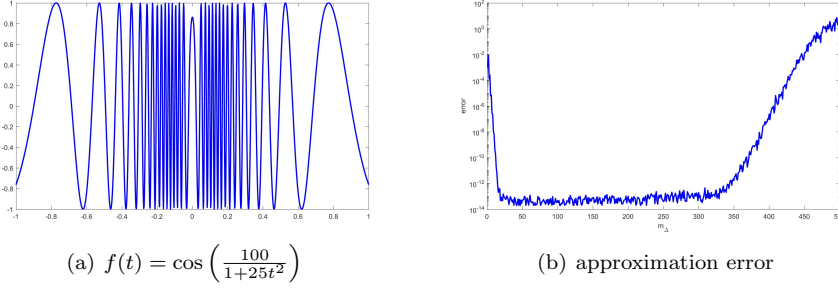


FIG. 5.7. The function and its approximation errors against  $m_\Delta$  for  $M = 500$ ,  $\gamma_\Delta = 1$ ,  $T_\Delta = 6$ .

calculation process is determined by the product  $(m_\Delta - 1)T_\Delta$ . When  $\gamma_\Delta \leq 1$ , the value of  $\hat{m}_\Delta$  at the corresponding  $\hat{T}_1$  is very close. When  $\gamma_\Delta > 1$ , the value of  $\hat{m}_\Delta$  at the corresponding  $\hat{T}_1$  increases rapidly with the increase of  $\gamma_\Delta$ . From the perspective of use, we are more concerned about the  $\hat{m}_\Delta$  value near  $\hat{T}_1$ . We tested this and the results are listed in Table 5.2.

It is also worth noting that for functions with internal oscillations but are smooth near the boundary, as mentioned in Section 5, an increase in the number of  $m_\Delta$  will cause the value of  $\omega$  in (4.8) to increase. If the value of  $M$  is not sufficiently large, the approximation result using a larger  $m_\Delta$  may be worse. This can be seen from the approximation results for the function  $f(t) = \cos\left(\frac{100}{1+25t^2}\right)$  in Fig. 5.7.

**5.3. Parameter determination.** Combining the test results in the previous two subsections, we know that if we want to approximate the function with frequency  $\omega$  with machine precision, the parameters  $T_\Delta$  and  $m_\Delta$  must satisfy

$$T_\Delta \geq \hat{T}_1, \quad m_\Delta \geq \hat{m}_\Delta. \quad (5.2)$$

Accordingly, combined with (5.1), the parameters  $L_\Delta$  and  $M$  must satisfy

$$L_\Delta \geq \hat{L}_\Delta =: 2 \times \hat{T}_1 \times \hat{m}_\Delta, \quad M \geq \hat{M} =: \hat{T}_1 \gamma_\Delta \omega. \quad (5.3)$$

Referring to the results in Table 5.1 and Table 5.2, the value of  $\hat{M}$  is very close for different  $\gamma_\Delta$  values, and the value of  $\hat{L}_\Delta$  is relatively close when  $\gamma_\Delta = 1$  and 2; however, the value of  $\hat{L}_\Delta$  is much larger when  $\gamma_\Delta$  takes other values. Further combined with the value of  $\hat{m}_\Delta$ , it can be seen that the computational complexity of the method is equivalent when  $\gamma_\Delta = 1$  and  $\gamma_\Delta = 2$ , whereas the computational complexity increases significantly in other cases. Furthermore, a larger  $m_\Delta$  indicates a greater probability of encountering high frequencies within the selected boundary interval. Therefore, we recommend using the following parameters

$$\gamma_\Delta = 1, T_\Delta = 6, m_\Delta = 25, \quad (5.4)$$

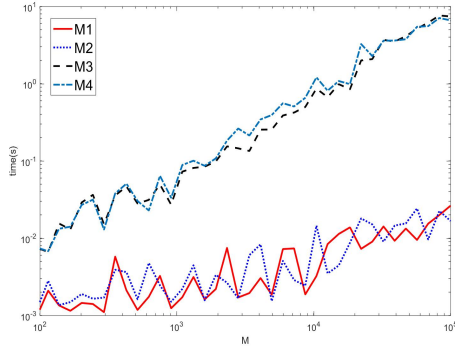


FIG. 6.1. Execution time for increasing the number of nodes  $M$ , for MATLAB implementations of the Boundary Interval algorithm (M1), the FC-Gram algorithm (M2), the Lyon algorithm (M3) and Implicit projection algorithm (M4).

for actual calculations, and parameters

$$\gamma_{\Delta} = 2, T_{\Delta} = 2.3, m_{\Delta} = 65, \quad (5.5)$$

can be used as an alternative. Under such parameter settings, the size of matrix  $A$  in (3.5) is small, and singular value decomposition can be calculated directly. In addition, note that  $A$  is fixed in the algorithm, so the SVD of  $A$  can be pre-computed and stored.

## 6. Testing and further improvement of the algorithm.

**6.1. Testing and comparison of algorithm performance.** Based on the previous tests, we have provided specific values for the parameters involved in the algorithm. In this subsection, the performance of the proposed algorithm is tested. All tests were computed on a Windows 10 system with 16 GB of memory, Intel(R) Core(TM)i7-8500U CPU1.80GHz using MATLAB 2016b. We compared the boundary interval algorithm (M1) proposed in this paper with the FC-Gram algorithm (M2) in [5], the Lyons algorithm (M3) in [12] and the implicit projection algorithm (M4) in [14]. For convenience of numerical implementation, for M3, we set parameters  $T = 2, \gamma = 2$ . For M4, we selected the best result from the three parameter combinations of  $T = 6, \gamma = 1$ ,  $T = 2, \gamma = 2$ , and  $T = 1.2, \gamma = 4$  (the performance of the three parameter combinations for different functions is slightly different. We also tested other parameter combinations and found that no combination with a product of  $T$  and  $\gamma$  less than 4 can achieve machine precision).

Algorithms M1 and M2 exhibit computational complexity of  $\mathcal{O}(M \log M)$ , in contrast to the  $\mathcal{O}(M \log^2 M)$  complexity inherent to algorithms M3 and M4. Figure 6.1 demonstrates the scaling behavior of execution time versus node count  $M$  across all four algorithms. These experimental observations align with the above conclusions: M1 and M2 demonstrate nearly identical temporal profiles, as do M3 and M4; for equivalent  $M$  values, M1/M2 achieve superior computational efficiency compared with M3/M4. It should be noted that  $M$  values required by these four algorithms are different. For M1/M2, the minimum  $M$  is governed by the approximation capacity of the boundary interval and maximum frequency of the approximated function. For full-data algorithms such as M3 and M4,  $M$  depends on both the function frequency

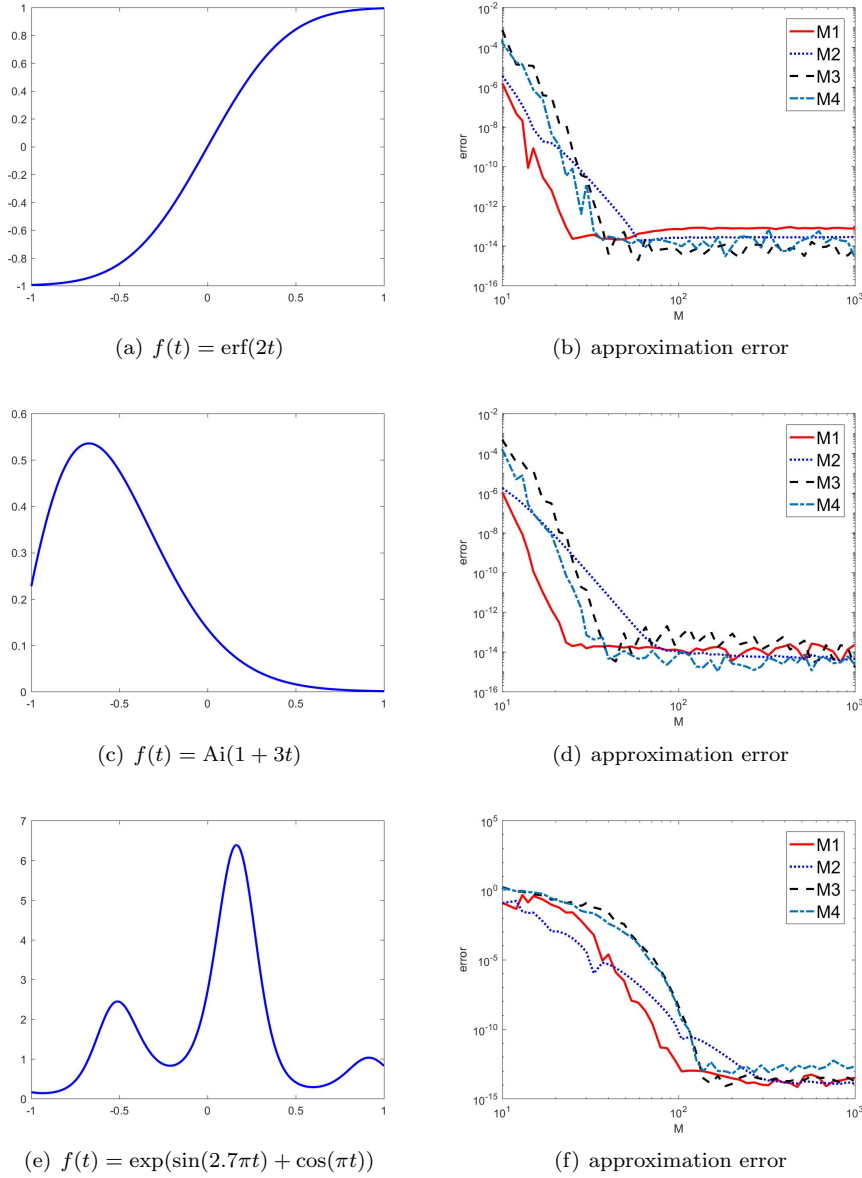


FIG. 6.2. Overall smooth functions and their approximation errors against  $M$ .

and the critical parameter product  $T\gamma$ . Notably, our empirical studies and existing literature establish  $T\gamma = 4$  as the minimum allowable value for full-data algorithms to attain machine precision. Subthreshold  $T\gamma$  values result in accuracy degradation for such methods.

The accuracy of the solution obtained using the four algorithms is shown in Fig. 6.2 - 6.4. To better show the differences, we divided the function into three cases for comparison:

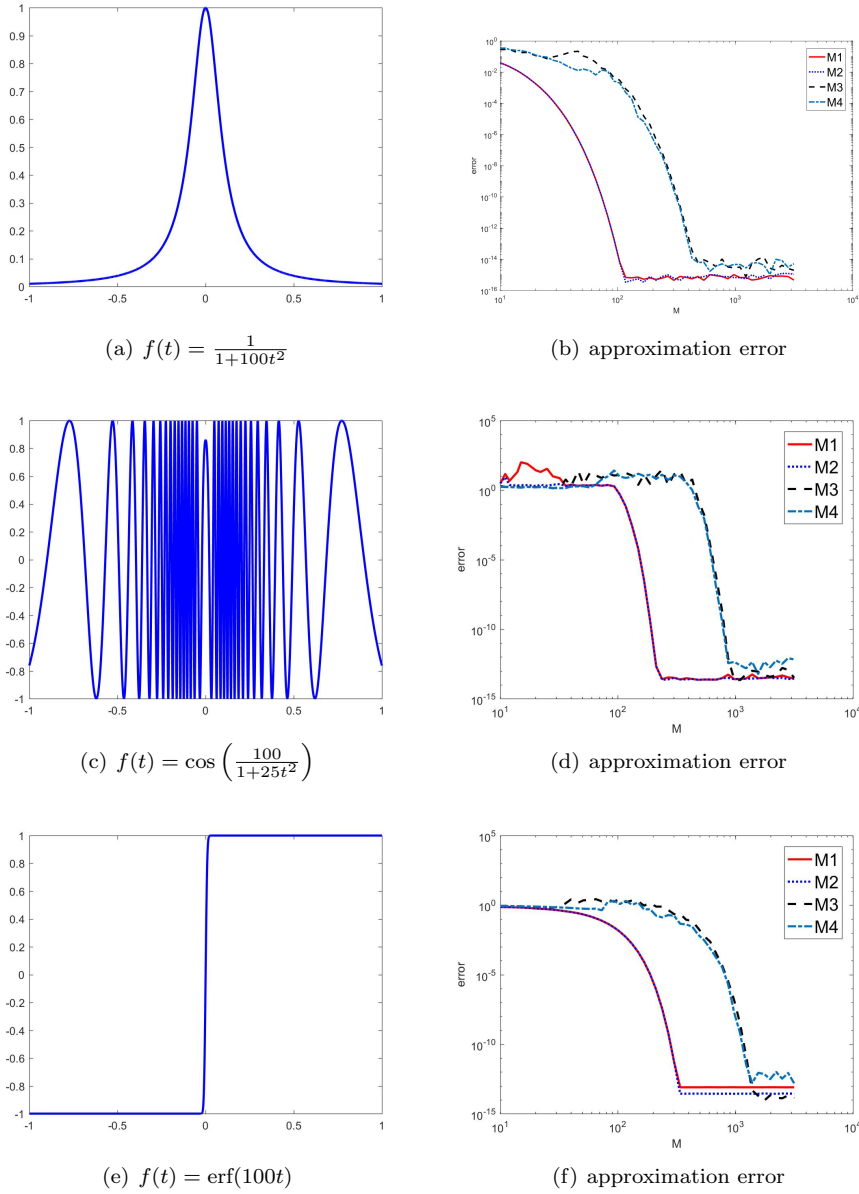


FIG. 6.3. Internal oscillating functions and their approximation errors against  $M$ .

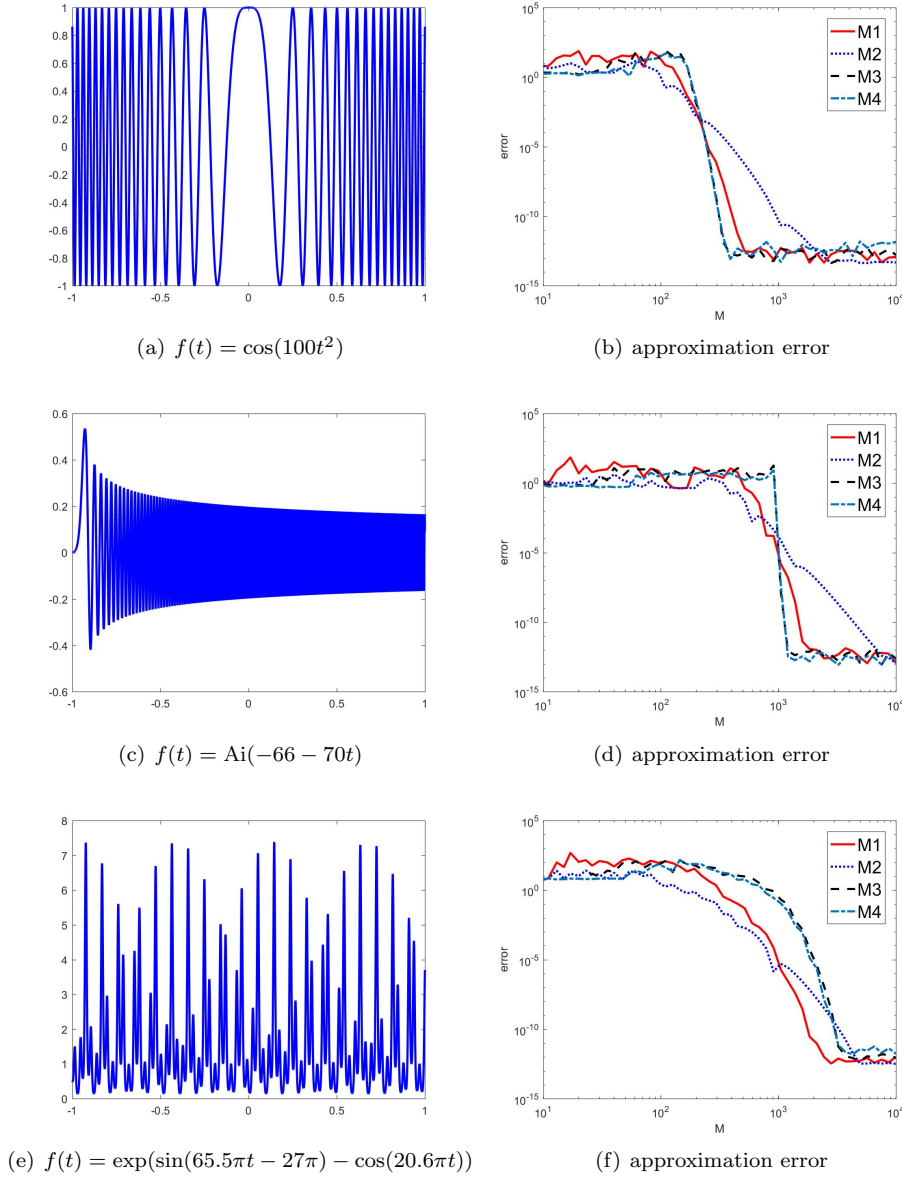
- Overall smooth functions:

$$f_1(t) = \text{erf}(2t), \quad f_2(t) = \text{Ai}(1 + 3t), \quad f_3(t) = e^{\sin(2.7\pi t) + \cos(\pi t)}.$$

- Internal oscillating functions:

$$f_4(t) = \frac{1}{1 + 100t^2}, \quad f_5(t) = \frac{100}{\cos(1 + 25t^2)}, \quad f_6(t) = \text{erf}(100t).$$




 FIG. 6.4. Boundary oscillating functions and their approximation errors against  $M$ .

- Boundary oscillating functions:

$$f_7(t) = \cos(100t^2), \quad f_8(t) = \text{Ai}(-66 - 70t), \quad f_9(t) = e^{\sin(65.5\pi t - 27\pi) - \cos(20.6\pi t)}.$$

Fig. 6.2 shows the numerical results for the first case. As mentioned above, the number of nodes  $M$  required for M1 and M2 is determined by the frequency of the boundary interval, but M2 cannot achieve superalgebraic convergence using polynomial approximation, so the value of  $M$  required is significantly larger than M1; while M3 and M4 are determined by the maximum frequency of the function

in the entire interval, and the number of nodes required is slightly larger than M1. At this time, the number of nodes  $M$  required by the four algorithms to achieve machine accuracy was relatively small, therefore, there was no obvious difference in performance.

In the second case, that is, when the function oscillates internally. As the frequency of the function in the boundary interval is much lower than that in the interior, the number of nodes required for M1 and M2 is determined by the resolution constant of the standard Fourier transform. Note that the resolution constants of M3 and M4 are  $T\gamma$ , so from (4.9) we can see that the number of nodes required for M1 and M2 is approximately 1/4 of that for M3 and M4, which is consistent with the results given in Fig. 6.3.

In the third case, because the function oscillates near the boundary, the algorithm in this paper cannot avoid this singularity. For functions  $f_7$  and  $f_8$ , the maximum frequency of the function appears in the boundary interval. According to (4.7), the number of nodes required by the proposed algorithm is  $T_\Delta\gamma_\Delta = 6$  times the maximum frequency, whereas the number of nodes required by M3 and M4 is  $T\gamma = 4$  times the maximum frequency. This is consistent with the results presented in Figures 2 and 3. For  $f_9$ , because the internal frequency is higher, the number of nodes required by the proposed algorithm is less than that of M3 and M4. As for M2, we can see that its approximation ability for the boundary interval data is obviously weaker than that of M1, therefore, more nodes are needed to achieve similar accuracy.

**6.2. Algorithm improvement: boundary grid refinement.** In certain situations, different step sizes may be used for interior and boundary sampling. The test results in the previous subsection indicate that the resolution constant is affected by the oscillation of the boundary interval data. This naturally raises the question: Can the algorithm performance be improved if a finer grid is used near the boundary than inside? In this section, we combine this concept to provide a modified algorithm for the boundary oscillation function.

Let  $R$  be a positive integer and

$$t_\ell^R = \frac{\ell}{RM}, \quad \ell = -RM, \dots, RM. \quad (6.1)$$

The positive integer  $m_\Delta^R$  denotes the number of nodes selected in the boundary interval. Notably, only  $2 \times m_\Delta^R$  nodes near the boundary were used in the actual calculation. The other nodes can be ignored, but they are listed here for convenience. For consistency with the boundary interval taken in the previous algorithm, we let

$$m_\Delta^R = R(m_\Delta - 1) + 1 \quad (6.2)$$

and

$$L_\Delta^R = 2 \times [T_\Delta \times (m_\Delta^R - 1)], \quad h^R = \frac{2\pi}{L_\Delta^R}, \quad x_j^R = (j-1)h, \quad j = 1, 2, \dots, L_\Delta^R. \quad (6.3)$$

Similarly, let

$$J_{\Delta,1}^R = \{1, 2, \dots, m_\Delta^R\}, \quad J_{\Delta,2}^R = \left\{ \frac{L_\Delta^R}{2} + 1, \frac{L_\Delta^R}{2} + 2, \dots, \frac{L_\Delta^R}{2} + m_\Delta^R \right\}, \quad J_\Delta^R = J_{\Delta,1}^R \cup J_{\Delta,2}^R. \quad (6.4)$$

and for  $j \in J_{\Delta}^R$ , take

$$g^R(x_j^R) = \begin{cases} f(t_{RM-m_{\Delta}^R+j}^R), & j \in J_{\Delta,1}, \\ f(t_{-RM+j-L_{\Delta}^R/2-1}^R), & j \in J_{\Delta,2}. \end{cases} \quad (6.5)$$

The extension function  $g_c^R(x_j^R)$ ,  $j = 1, 2, \dots, L_{\Delta}^R$  was also obtained according to the method described in section 3. And then we obtain a function  $f_c^R$  with a period of  $2 + \lambda$ , where  $\lambda$  is same as in (2.6). The data of the extension function  $f_c^R(t_{\ell})$ ,  $\ell = -M, \dots, M, M+1, \dots, M + \lceil T_{\Delta} - 1 \rceil \times (m_{\Delta} - 1) - 1$  in one period  $[-1, 1 + \lambda)$  are

$$f_c^R(t_{\ell}) = \begin{cases} f(t_{\ell}), & |\ell| \leq M, \\ g_c^R(x_{m_{\Delta}^R+(\ell-M) \cdot R}), & \ell > M. \end{cases} \quad (6.6)$$

The original algorithm is equivalent to a special case of the improved algorithm when the parameter  $R = 1$ .

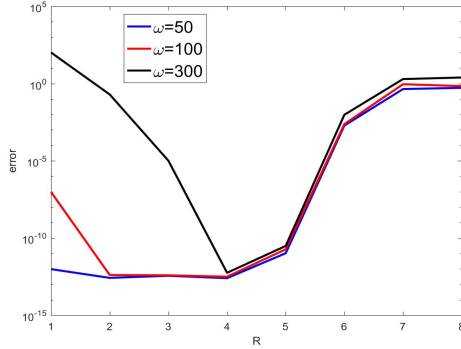


FIG. 6.5. The approximation error against  $R$  for functions  $\exp(i\omega\pi t)$ ,  $M = 500$ .

Now we take  $\gamma = 1, T_{\Delta} = 6, m_{\Delta} = 25$  to test the influence of parameter  $R$  on the algorithm. As can be seen from Fig. 6.5, when  $R \geq 5$ , the approximation error not only does not improve, but becomes worse, which is caused by the instability of the calculation of the extension part. When  $R \leq 4$ , it can be observed that the refinement of grid near the boundary improves the approximation error. When  $\omega = 50$ , the improvement is not obvious, because the number of nodes  $M = 500 > T_{\Delta}\gamma_{\Delta}\omega$  has exceeded the threshold for resolving this frequency function. Therefore, when facing high-frequency functions, we recommend using parameters

$$\gamma_{\Delta} = 1, T_{\Delta} = 6, m_{\Delta} = 25, R = 4$$

for calculation.

Next, we tested the performance of the improved algorithm (M5) and compared it with the original algorithm (M1). We selected several test functions with significant high-frequency features in the boundary interval:

$$f_{10}(t) = \frac{1}{1.01 - t^2}, \quad f_{11}(t) = \text{Ai}(150t), \quad f_{12}(t) = \sin(1500t^2).$$

Fig. 6.6 shows the graphs of the test functions and the corresponding approximation results. We can see that the refinement of grid near the boundary effectively

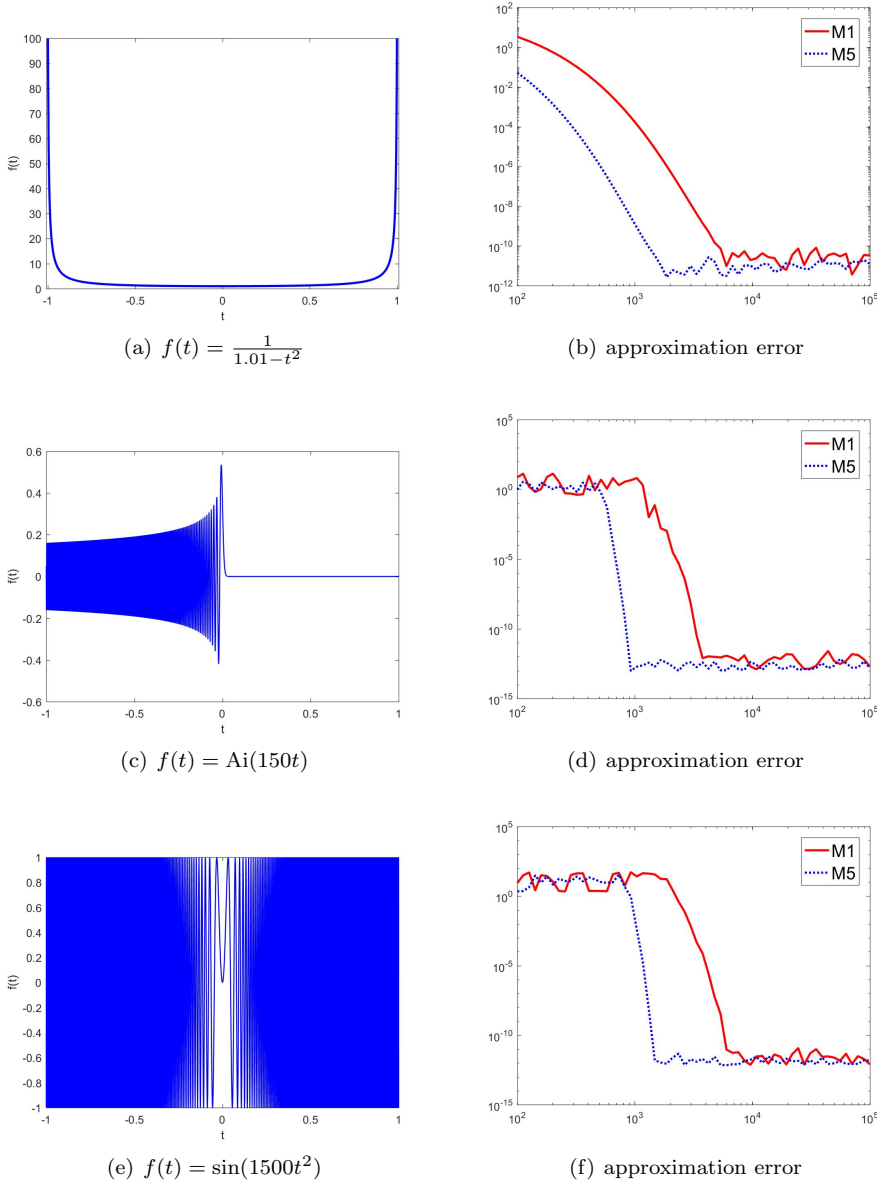


FIG. 6.6. Comparisons of algorithms  $M1$  and  $M4$ .

reduces the resolution constant. The number of nodes required to achieve machine accuracy in the improved method was approximately  $1/4$  of that in the original method.

**7. Conclusions.** Fast algorithms based on boundary interval data has been proposed for the computation of the Fourier extension approximation to nonperiodic functions. We tested the relevant parameters and provided the setting scheme. The new algorithms have a computational complexity of  $\mathcal{O}(M \log(M))$  and can be used as basic tools for the calculation of the Fourier extension.

**Acknowledgments.** The authors would like to sincerely thank Mark Lyon for generously sharing the MATLAB codes in [5] and [12] to facilitate comparative analysis in this work.

## REFERENCES

- [1] B. ADCOCK AND D. HUYBRECHS, *On the resolution power of Fourier extensions for oscillatory functions*, Journal of Computational and Applied Mathematics, 260 (2014), pp. 312–336.
- [2] B. ADCOCK, D. HUYBRECHS, AND J. MARTÍN-VAQUERO, *On the numerical stability of Fourier extensions*, Foundations of Computational Mathematics, 14 (2014), pp. 635–687.
- [3] B. ADCOCK AND J. RUAN, *Parameter selection and numerical approximation properties of Fourier extensions from fixed data*, Journal of Computational Physics, 273 (2014), pp. 453–471.
- [4] J. P. BOYD, *A comparison of numerical algorithms for Fourier extension of the first, second, and third kinds*, Journal of Computational Physics, 178 (2002), pp. 118–160.
- [5] O. P. BRUNO AND M. LYON, *High-order unconditionally stable FC-AD solvers for general smooth domains I. basic elements*, Journal of Computational Physics, 229 (2010), pp. 2009–2033.
- [6] O. P. BRUNO AND J. PAUL, *Two-dimensional Fourier continuation and applications*, SIAM Journal on Scientific Computing, 44 (2022), pp. A964–A992.
- [7] T. A. DRISCOLL AND B. FORNBERG, *A Padé-based algorithm for overcoming the Gibbs phenomenon*, Numerical Algorithms, 26 (2001), pp. 77–92.
- [8] J. GEER, *Rational trigonometric approximations to piece-wise smooth periodic functions*, Journal of Scientific Computing, 10 (1995), pp. 325–356.
- [9] A. GELB AND J. TANNER, *Robust reprojection methods for the resolution of the Gibbs phenomenon*, Applied and Computational Harmonic Analysis, 20 (2006), pp. 3–25.
- [10] D. GOTTLIEB, C. W. SHU, A. SOLOMONOFF, AND H. VANDEVEN, *On the Gibbs phenomenon i: recovering exponential accuracy from the Fourier partial sum of a nonperiodic analytic function*, Journal of Computational and Applied Mathematics, 43 (1992), pp. 81–98.
- [11] D. HUYBRECHS, *On the Fourier extension of nonperiodic functions*, SIAM Journal on Numerical Analysis, 47 (2010), pp. 4326–4355.
- [12] M. LYON, *A fast algorithm for Fourier continuation*, SIAM Journal on Scientific Computing, 33 (2011), pp. 3241–3260.
- [13] ———, *Sobolev smoothing of SVD-based Fourier continuations*, Applied Mathematics Letters, 25 (2012), pp. 2227–2231.
- [14] R. MATTHYSEN AND D. HUYBRECHS, *Fast algorithms for the computation of Fourier extensions of arbitrary length*, SIAM Journal on Scientific Computing, 38 (2016), pp. A899–A922.
- [15] ———, *Function approximation on arbitrary domains using Fourier extension frames*, SIAM Journal on Numerical Analysis, 56 (2018), pp. 1360–1385.
- [16] G. PLONKA, D. POTTS, G. STEIDL, AND M. TASCHE, *Numerical Fourier Analysis*, Springer, 2018.
- [17] E. M. STEIN AND R. SHAKARCHI, *Fourier Analysis: An Introduction*, Princeton University Press, New Jersey, 2003.
- [18] J. TANNER, *Optimal filter and mollifier for piecewise smooth spectral data*, Mathematics of Computation, 75 (2006), pp. 767–790.
- [19] A. N. TIKHONOV, A. V. GONCHARSKY, AND A. G. STEPANOVA, V. V. YAGOLA, *Numerical Methods for the Solution of Ill-posed Problems*, Kluwer Academic Publishers, Dordrecht, 1995.
- [20] Y. F. WANG, I. E. STEPANOVA, V. N. TITARENKO, AND A. G. YAGOLA, *Inverse Problems in Geophysics and Solution Methods*, Higher Education Press, Beijing, 2011.
- [21] M. WEBB, V. COPPÉ, AND D. HUYBRECHS, *Pointwise and uniform convergence of Fourier extensions*, Constructive Approximation, 52 (2020), pp. 139–175.